JACS
JOURNAL OF THE AMERICAN CHEMICAL SOCIETY
Article
pubs.acs.org/JACS

The Nucleation and Growth Mechanism of Thiolate-Protected Au Nanoclusters

Chunyan Liu,[†] Yong Pei,*[,‡] Hui Sun,[†] and Jing Ma*[,†]

[†]Key Laboratory of Mesoscopic Chemistry of MOE, School of Chemistry and Chemical Engineering, Nanjing University, 22 Hankou Road, Nanjing, Jiangsu Province 210093, People's Republic of China

[‡]Department of Chemistry, Key Laboratory of Environmentally Friendly Chemistry and Applications of MOE, Xiangtan University, Xiangtan, Hunan Province 411105, People's Republic of China

Supporting Information

ABSTRACT: The understanding of the evolution mechanism of thiolate-protected Au nanoclusters from the homoleptic Au(I)-SR clusters to core-stacked ones is crucial for the synthesis of novel thiolated Au clusters. In this work, the global search for a series of "intermediate" $Au_m(SR)_n$ clusters with m and n ranging from 5 to 12 was implemented by combining basin hopping algorithm, genetic algorithm, and density functional theory (DFT) calculations. Most of $Au_m(SR)_n$ clusters possess the core−shell structure. Specifically, some typical topologies, such as tetrahedral Au_4, triangular bipyramid Au_5, octahedral Au_6, and vertex-shared Au_7, are found to be dominant within the inner core of various clusters. Along with the increase in the number of gold atoms and thiolates, the preliminary nucleation and growth processes of both inner-core and staple-motif protecting units are grouped into three kinds of size evolution routes, i.e., core growth, core dissolution, and staple-motif growth, respectively. Some metastable isomers may also play an important role in the evolution of clusters. The core structures in the lowest-lying isomers and some metastable isomers are similar to the intact or part of the cores found in experimentally detected species. Both the lowest-lying and metastable intermediate clusters may serve as the building block for the further growth. These results rationalize the preliminary nucleation in the "reduction growth" stage, shedding light on the size-evolution mechanism of RS-AuNPs.

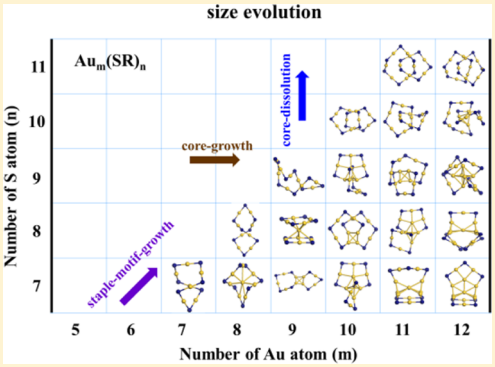

1. INTRODUCTION

The thiolate-protected gold nanoparticles $Au_m(SR)_n$ (denoted as RS-AuNPs) exhibit extensive potential in diverse fields like biosensor and catalysis.[1−5] To make good use of this material, it is imperative to synthesize monodisperse clusters with varying atomic composition on a large scale and determine the precise atomic structures as well as the properties.[3,6−8] In experiments, a series of monodisperse RS-AuNPs such as $Au_{102}(SR)_{44}$ and $Au_{25}(SR)_{18}^-$, etc. have been successfully characterized through XRD.[9−21] Based on these structures, the intrinsic rules of thiolate-protected Au nanoclusters have been summarized, leading to the predictions of several structurally unresolved clusters.[22] Also, the explanation of the stability has been achieved by using "superatom" and "superatom network" concepts.[23,24]

The synthesis of RS-AuNPs based on the conventional bottom-up strategy consists of three stages in experiment: (i) the reaction of $HAuCl_4$ and thiolate ligand leading to Au(I)-SR oligomer; (ii) the reduction of Au(I)-SR to a number of mixed small-sized $Au_m(SR)_n$ ($m > n$) intermediates; and (iii) a size-focusing process in which only the clusters with higher stability survive.[25] The final product is highly sensitive to the reaction conditions such as temperature, solvent, reducing reagent, and so on.[7,8,26,27]

Recently, the structure of $Au_{15}(SR)_{13}$ was predicted to possess a Au_4 tetrahedron inner core and cyclic $Au_5(SR)_5$ protecting unit, which could be viewed as the intermediate from homoleptic Au(I)-SR complex to normal core-stacked clusters.[28] Xie and co-workers traced the possible intermediates in the synthesis of $Au_{25}(SR)_{18}$ to investigate the nucleation and growth mechanism by using CO as reducing reagent to slow down the reaction. A series of small-sized AuNC intermediates were identified through ESI-MS.[29,30] However, the explicit size-evolution mechanism in the different reaction stages is still vague, and it comes down to the lack of information on the intermediates between homoleptic $Au_m(SR)_m$ clusters and experimentally resolved ones.

Here, we performed a systematic global structure search on a series of intermediate $Au_m(SR)_n$ with m and n ranging from 5 to 12, from which a general nucleation and growing process for both inner cores and outer protecting units is observed along with the size increment. The structure of cluster is found to be notably sensitive to the number of the Au and SR, especially the type of Au core. More importantly, by comparing these small-sized "intermediates" with the experimentally resolved core-

Received: September 7, 2015
Published: November 25, 2015

DOI: 10.1021/jacs.5b09466
J. Am. Chem. Soc. 2015, 137, 15809−15816

stacked clusters ("product"), the discovered inner Au_4, Au_6 and Au_7 cores of the energetically lowest-lying isomers and some metastable isomers possess high similarity with cores of the known clusters. This discovery suggests that not only the lowest-lying transition clusters but also some metastable ones may serve as the building block for the next growth stage and thereby possess the ability to affect the final product.

2. COMPUTATIONAL METHOD AND DETAILS

A large number of low-energy isomers for each cluster were generated through a global search algorithm and subsequently optimized using density functional theory (DFT). In order to search the minimum structure more efficiently, we associated the basin-hopping algorithm with a genetic algorithm. Basin-hopping algorithm transforms the rough potential energy surface (PES) to a number of basins and explores the whole PES through Monte Carlo random moves that are accepted with certain probability based on the Metropolis criterion.[31] Basin-hopping algorithm usually works well for the rapid searching of global minimum structures of small-to-medium-sized atomic clusters. However, in certain cases, such as $Au_{12}(SR)_{11}$, the searching is easily trapped in some deep valleys in the PES, which significantly hinders the efficiency and possibility of finding the real global minimum. To avoid this drawback, we combined genetic algorithm by using the local minimums primarily searched by the basin-hopping as the initial individuals in the following search. Genetic algorithm is an evolution algorithm based on the population, which generates the new individuals by applying the crossover and mutation operation to the parent populations and achieves a better offspring according to the "survival of the fitness" principle.[32] Moreover, considering the computational accuracy and efficiency, the PBE/DND4.4 basis set together with the semicore pseudopotential in the DMol^3 package were chosen in the structural optimization.[33−35] With the combination of the basin-hopping algorithm and genetic algorithm, we picked out the global minimum and some energetically degenerate or higher-lying metastable isomers to further draw the evolution trend of "intermediate" $Au_m(SR)_n$ from the initial homoleptic ones ("precursor") to the final core-stacked ones. In the first step of understanding the size-evolution trend in cluster growth, the simplified model −SH was employed to represent the −SR group in the search of local minima. The other two kinds of functional groups of $-SCH_3$ and $-SC_6H_4$-*m*-COOH (*m*-MBA) were then selected to study the ligand influence on the relative stabilities of the RS-AuNPs.

3. RESULTS AND DISCUSSION

3.1. The Size Evolution of RS-AuNPs in Reduction Nucleation Stage. Based on the aforementioned algorithm and computational methods, the systematic global structure search was carried out one by one along with continuously increasing the number of gold atoms and thiolates, and the energetically low-lying isomers for each cluster were summarized in Figure 1a. The structures of homoleptic $Au_m(SR)_m$ clusters with *m* ranging from 6 to 12 have been reported in the previous reference.[36] The optimized geometries and electronic energies of other $Au_m(SR)_n$ clusters are displayed in Supporting Information. With the addition of more gold atoms and thiolate groups to the initial homoleptic clusters, the core-stacked framework is formed, which exhibits several interesting trends. Basically, the growth of inner core follows the same trend evolving from the initial Au_2 to smaller Au_3, Au_4, and then to the Au_5, Au_6 cores, etc., as shown in Figure 1b. Furthermore, based on the located minimum structures of various $Au_m(SR)_n$ clusters, we summarized three kinds of growth pathways, i.e., core growth, core dissolution, staple-motif growth, as manifested in Figure 1a by different colored arrows.

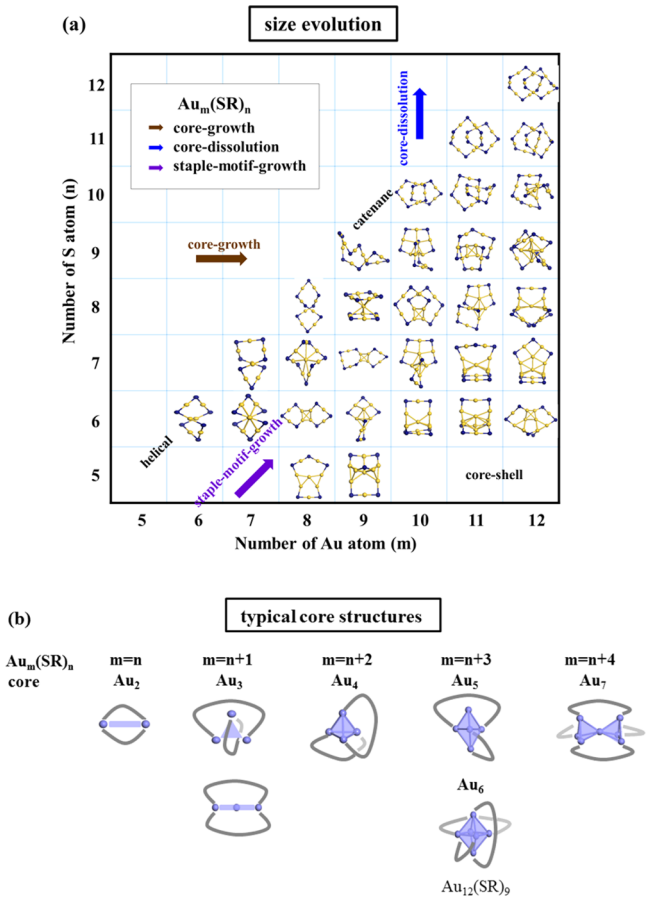

Figure 1. Schematic illustrations of (a) the size-evolution of $Au_m(SR)_n$ clusters and (b) the core−shell structure with various typical inner cores. Yellow and blue balls represent Au and S atoms, respectively, and the −H groups bonded to S are eliminated for clarity.

Concerning the formula $Au_m(SR)_m$ (dissolved as $Au_2[Au_{(m-2)/2}(SR)_{m/2}]_2$ or $Au_2[Au_{(m-3)/2}(SR)_{(m-1)/2}][Au_{(m-1)/2}(SR)_{(m+1)/2}]$) and the corresponding structures, each different sized homoleptic RS-AuNPs can be viewed as the Au_2 inner core protected by staple motifs with varied length. Starting from the "precursor", the continuously added Au atoms tend to fill in the Au core, and the bigger inner cores are generated with the outer ligands remaining the same. It is worth noting that the growth of Au cores from diverse "precursors" basically follows the same evolution pattern as demonstrated in Figure 1b. The triangular Au_3 or linear Au_3 and tetrahedral Au_4 cores are formed after the addition of one and two Au atom(s). When three Au atoms are added, both triangular bipyramid Au_5 and octahedral Au_6 cores are observed. Furthermore, a vertex-shared bitetrahedron Au_7 core is formed with an addition of four Au atoms.

In addition, the average connectivity of Au atom in each intermediate cluster is calculated, and the definition of the connectivity is given in Supporting Information (SI). Because the Au atoms in the inner core usually own higher connectivity than those in the staple motif, the calculation of average connectivity of Au atoms in each cluster could represent the nucleation degree of each cluster. The larger value of connectivity indicates a higher degree of nucleation. For each core-growth route starting from different homoleptic species, the average connectivity of the Au atoms generally exhibits an increasing trend as illustrated in Figure 2a and implies a larger

DOI: 10.1021/jacs.5b09466
J. Am. Chem. Soc. 2015, 137, 15809−15816

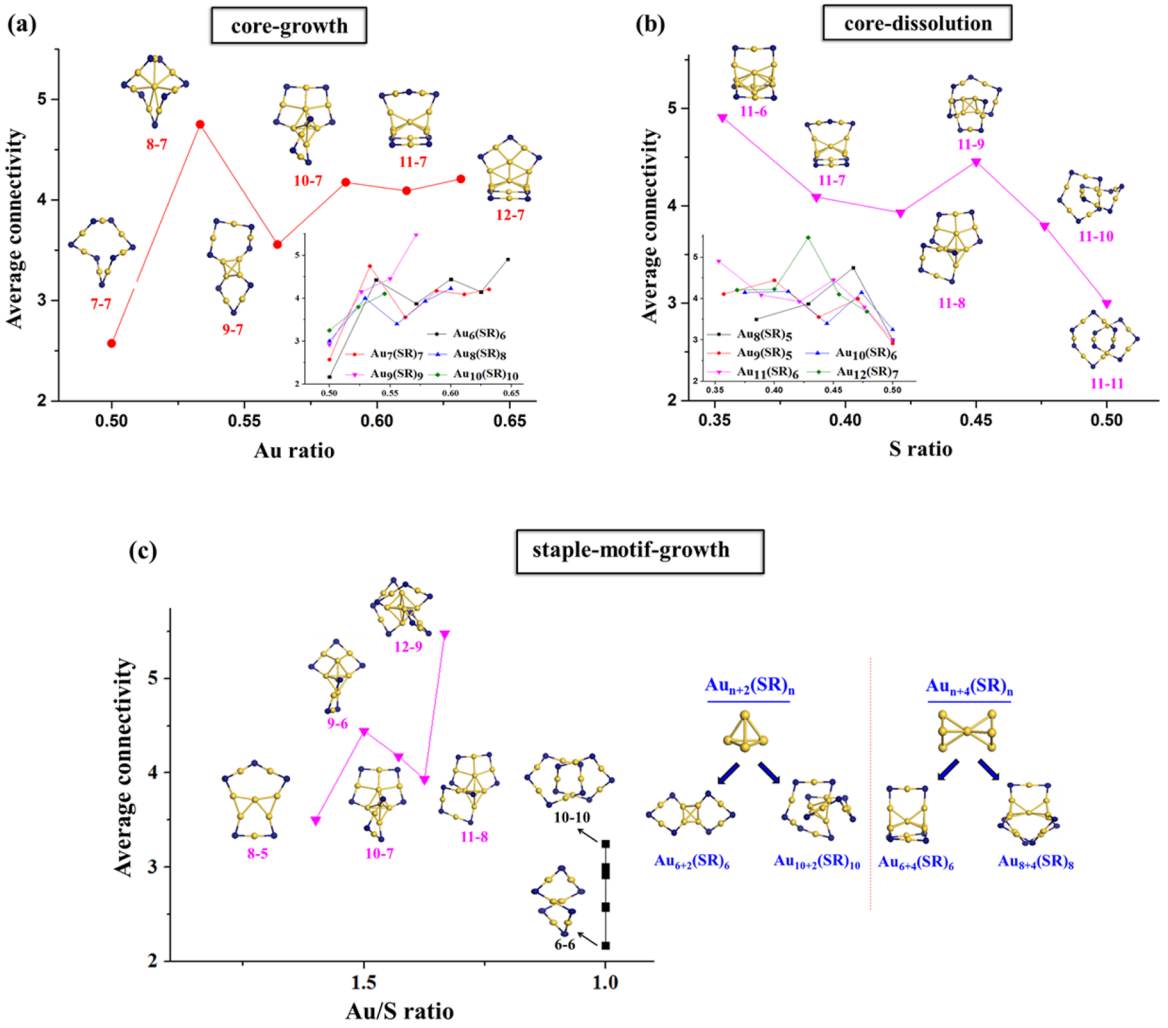

Figure 2. Average connectivity along (a) core-growth route starting from different homoletpic clusters; (b) core-dissolution routes starting from different core-stacked clusters; and (c) staple-motif growth route starting from different clusters.

extent of nucleation. In fact, the assembly pattern of the staple motif depends on both the length of the staple motif and the structure of the core. Specifically, the dimer motif in $Au_8(SR)_6$ can only protect the edge of the Au_4 core, leading to a longer distance between gold atoms in the inner cores and in the staple motifs than the Au···Au distance in $Au_7(SR)_6$, and hence the decrease in the average connectivity of Au. Thereby, in some cases, the growth on core may associate with the decline of the connectivity. Both the optimized structure and average connectivity depict the trend of preliminary nucleation from circular homoleptic RS-AuNPs to core-stacked RS-AuNPs for the first time, which is called the core-growth route in this work.

Compared with the core-growth route, an added thiolate tends to invade the Au−Au bond and connects two adjacent Au atoms in the inner core, leading to the increase of the outer staple motif and simultaneous diminution of the core. This route (denoted as the core-dissolution route) is somewhat similar to the "dissolution" of the inner core ("solute") with increasing thiolates ("solvent"), as shown by the blue arrow in Figure 1a. More specifically, Figure 2b describes the gradual "dissolution" of the core and the decreasing trend of the connectivity along each core-dissolution path. For example, the detailed evolution process of the structures starting from $Au_{11}(SR)_6$ cluster (with Au_8 core) to $Au_{11}(SR)_{11}$ without core is highlighted in Figure 2b, in which a vivid "melt" or "dissolution" course from the large Au_8 core to the Au_2 core is observed with the addition of thiolates one by one.

If the core-growth and core-dissolution routes are coupled together, namely, the simultaneous addition of a single Au atom and a thiolate, the same inner core with elongated staple motif is formed. This process is displayed as the staple-motif-growth route in purple arrow within Figure 1a. Intriguingly, along the staple-motif route, the type of the inner core is controlled by the value of difference between m and n. The $Au_{n+2}(SR)_n$ or $Au_{n+4}(SR)_n$ clusters can be decomposed as the tetrahedral Au_4 core or vertex-sharing bitetrahedral Au_7 core capped by the staple motifs with varied lengths, as shown in Figure 1b and Figure 2c. Among them, $Au_{12}(SR)_9$ can be taken as an exception, which owns a Au_6 octahedral core rather than the triangular bipyramid Au_5 core, similar to the structure predicted by Jiang.[37] For a Au_6 octahedral core, three longer second-length staple motifs are needed to achieve the flawless protection, while the short first-length staple motif leads to considerable deformation. As a result, the structure of $Au_{12}(SR)_9$ appears to be a compromise between the octahedral Au_6 inner core and the outer protecting unit. For Au_7 vertex-sharing bitetrahedron core, the single thiolate and first-length

DOI: 10.1021/jacs.5b09466
J. Am. Chem. Soc. 2015, 137, 15809−15816

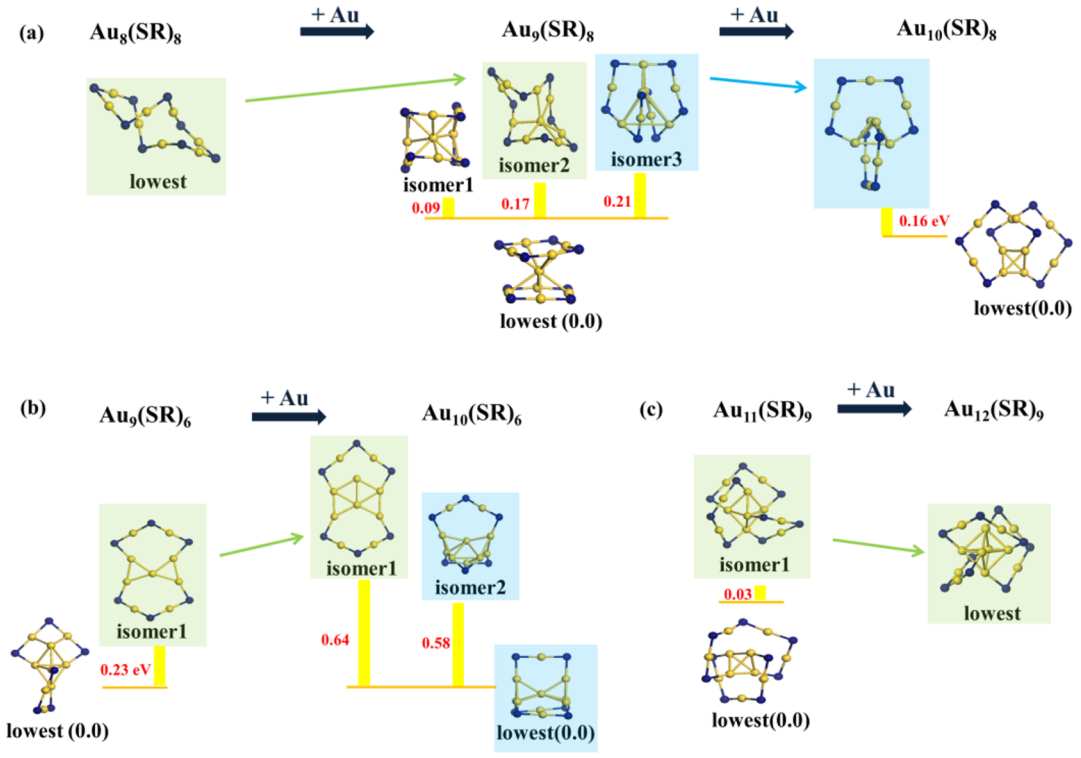

Figure 3. Illustration of metastable transition route for (a) $Au_8(SR)_8$ to $Au_9(SR)_8$, (b) $Au_9(SR)_6$ to $Au_{10}(SR)_6$, and (c) $Au_{11}(SR)_9$ to $Au_{12}(SR)_9$.

staple motif is sufficient. Correspondingly, the Au_7 core is formed as small as that in $Au_9(SR)_5$. In short, the favored structure of the cluster is more like the balance between the atom number and the Au/S ratio.

Most of the growth paths between different sized clusters obey the three above-mentioned rules, yet there are some exceptions, such as the conversion from $Au_8(SR)_8$ to $Au_9(SR)_8$, $Au_9(SR)_6$ to $Au_{10}(SR)_6$, $Au_{11}(SR)_9$ to $Au_{12}(SR)_9$, etc. The abnormality mainly appears at the striking transformation of Au inner core. However, if we look into the energetically low-lying isomers other than the global minimum for each clusters, some low-lying metastable isomers often possess the similar structure pattern between two neighboring clusters (Figure 3). It should be mentioned that the PES of cluster is very smooth, and the energy difference between the global minimum and some low-lying isomers is rather small. It is plausible that the structural evolution between different sized clusters may also take place through some pathways connecting those metastable isomers first and then to the global minima.

For example, as illustrated in Figure 3a, $Au_8(SR)_8$ exhibits a helical configuration, while the lowest-lying minimum of $Au_9(SR)_8$ is a structure (called X-cone-shaped) with two $Au_4(SR)_4$ ring linked to the same Au atom through Au−Au interaction. Such notable difference in structure causes the difficulty in the evolution from the helical $Au_8(SR)_8$ to the lowest-lying $Au_9(SR)_8$ through the direct addition of an extra gold atom. However, the higher energy minimum, isomer 2, of $Au_9(SR)_8$ bears considerable resemblance with $Au_8(SR)_8$. Thus, $Au_9(SR)_8$ cluster may be formed with the direct filling of an Au atom in the center of $Au_8(SR)_8$. Subsequently, starting from the isomer 2 of $Au_9(SR)_8$, the minor adjustment on the central Au atom as well as $Au_4(SR)_4$ ring will lead to formation of isomer 1, and the following motion of two Au atom of isomer 1 may give rise to the generation of the lowest-energy isomer of $Au_9(SR)_8$. Besides, when the continuous addition of a gold atom to the isomer 3 of $Au_9(SR)_8$, the isomer 1 of $Au_{10}(SR)_8$ is formed with the bottom two SR ligands being bridged by the added Au atom. The same circumstance also occurs in some other cases such as the growth from $Au_9(SR)_6$ to $Au_{10}(SR)_6$ and $Au_{11}(SR)_9$ to $Au_{12}(SR)_9$, according to similar structural framework of metastable isomers in Figure 3b,c. On the grounds of the above-mentioned examples, it is evident that the metastable isomers provide considerable assistance in the size-evolution of RS-AuNPs, and those higher energy pathways are hence called as the metastable-transition routes. In fact, the metastable state is taken as the "active species" in many cases such as the catalysis, phase transition, polymorph transformation, etc.

On the basis of aforementioned four different routes, we can demonstrate the preliminary nucleation phenomena from diverse homoleptic gold thiolates to core-stacked clusters and the further growth on both Au inner core and outer staple motifs with the increase of Au atoms and thiolates. Such a growth path is favored according to the increasing binding energy (E_b) along with the increment of atom, as shown in Figure S1. The size-independent relative stability of $Au_m(SR)_n$ cluster is also estimated by the average binding energy, $E_b/(m + n)$ in Figure S1. It is interesting to notice from Table S1 and S2 that the 2 e^- (i.e., $m = n + 2$) and 4 e^- ($m = n + 4$) systems have larger average binding energies than the other clusters. These computational results echo the initial 2 e^- reduction-growth process from Au(I)-SR to Au_{10-15} NCs, in which the 2 e^- clusters, $Au_{11}(SR)_9$ and $Au_{15}(SR)_{13}$, were identified as the intermediates.[29,30] One possible formation process of $Au_{11}(SR)_9$ was proposed to start from the reduction of $Au_6(SR)_6$ by CO to $Au_6(SR)_4$, and subsequent collision with $Au_5(SR)_5$.[29] Such a formation process is depicted as path 2 in Figure 4. After removing two ligands from $Au_6(SR)_6$, the new

DOI: 10.1021/jacs.5b09466
J. Am. Chem. Soc. 2015, 137, 15809−15816

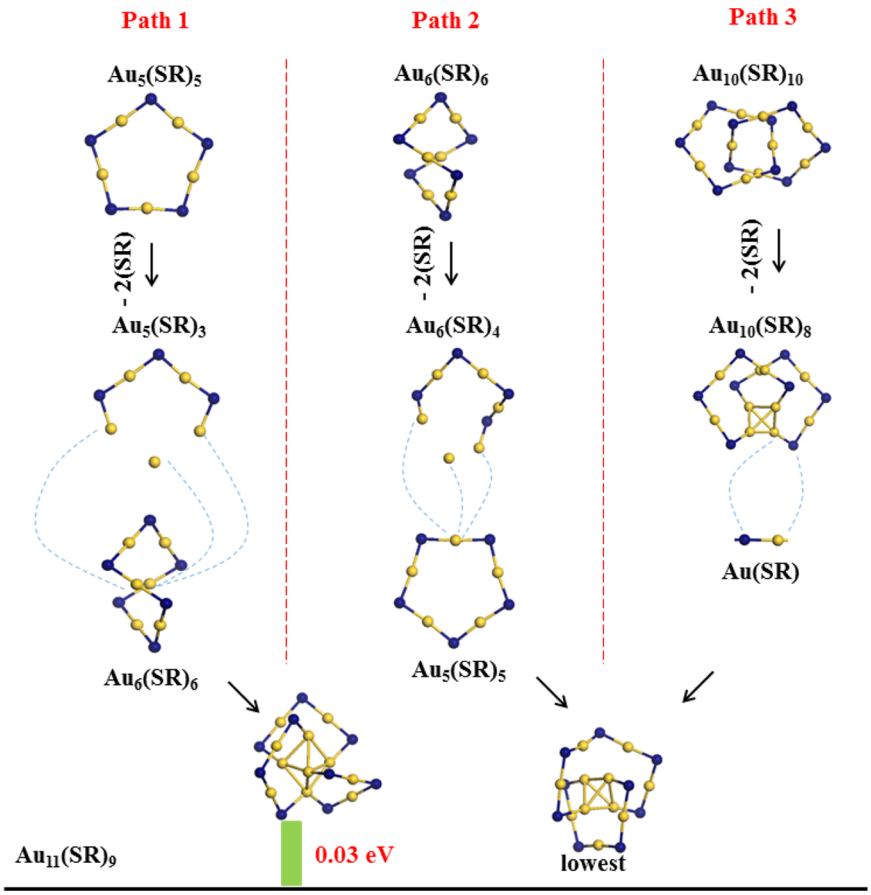

Figure 4. Three possible paths for the formation of $Au_{11}(SR)_9$.

$Au_6(SR)_4$ could be viewed as $Au_3[Au_3(SR)_4]_1$, namely, a Au_3 inner core protected by the trimer staple motif. Meantime the $Au_5(SR)_5$ could be decomposed as a single Au atom covered by the tetramer staple motif. Therefore, the fusion of $Au_6(SR)_6$ and $Au_5(SR)_5$ may cause the fusion of Au_3 and Au_1 cores in two clusters and give rise to a stable Au_4 tetrahedron unit. The resultant geometry from the above reduction collision and fusion resembles the geometry of lowest-lying $Au_{11}(SR)_9$ isomer. Alternatively, in the case that $Au_5(SR)_5$ is reduced first and collided with $Au_6(SR)_6$, the path 1 in Figure 4 demonstrates another possible fusion mode. In addition, given the existence of $Au_{10}(SR)_{10}$ and Au(SR), the $Au_{11}(SR)_9$ is also likely formed through the reduction of $Au_{10}(SR)_{10}$ and the following addition of Au(SR), as shown in path 3 of Figure 4. All three paths are feasible according to the geometry resemblance as well as the thermodynamics of reactions, although the paths through $Au_{10}(SR)_{10}$ and Au(SR) are more exothermic by about 28 kcal/mol, as shown in the Supporting Information. On the other side, the Au(0) and thiolate were probably generated from the reduction of existed $Au_2(SR)_2$, which may give rise to gradual growth on the Au(I) precursor as shown in Figure 1. The nucleation phenomenon is observed in all those possible pathways, which is helpful to understand the initial reduction-growth formation process. It should be mentioned that the reaction is sensitive to the condition, so some other intermediates may exist under different reaction conditions in spite of the similar growth pattern.

Notably, the structures of a number of Au_mS_n binary clusters (without −R group bonded to the S atom) in the same size were predicted to possess the hollow polyhedral pattern without center core and follow a "edge-to-face" growth pattern.[38] The structural difference between two types of clusters illustrates the importance of the outer ligand in controlling the structure and the related properties of the Au clusters. In addition, this preliminary nucleation and size-evolution process rationalizes the reduction-growth stage in experiment, in which the Au(I)-SR "precursors" are reduced to a narrow size distribution of "intermediates".

3.2. The Building Blocks for the Further Growth. The above discussions of growth mechanisms of small sized $Au_m(SR)_n$ clusters proposed that the tetrahedral Au_4, the vertex-sharing Au_7 and the octahedral Au_6 cores represent the common structural motifs of golden core of $Au_m(SR)_n$ clusters. In fact, we find that these golden core units also act as the basic building units of Au cores in larger-sized gold clusters such as $Au_{20}(SR)_{16}$, $Au_{25}(SR)_{18}^-$, $Au_{28}(SR)_{20}$, and $Au_{36}(SR)_{24}$, etc. In other words, most Au cores in "product" can be viewed as the combination of different numbers of Au_4−Au_7 cores as shown in Figure 5a. For instance, the $Au_{20}(SR)_{16}$ possesses the similar but slightly twisted Au_7 core as $Au_{10}(SR)_6$, while the Au inner core of $Au_{28}(SR)_{20}$ can be viewed as the assembly of two Au_7 core via aurophilic interaction. Besides, four tetrahedron Au_4 cores can form the icosahedron Au_{13} core of $Au_{25}(SR)_{18}$ by sharing the same central vertex, and in meantime two octahedron Au_6 core could share the common triangular face and constitute the Au_9 core in $Au_{18}(SR)_{14}$. The Au_9 core in $Au_{18}(SR)_{14}$ could also be generated by the addition of an extra Au atom on the Au_8 core in the metastable isomers of $Au_{11}(SR)_6$ and $Au_{12}(SR)_7$ (given in the SI). Moreover, the inner part in $Au_{23}(SR)_{16}$ is composed of two Au_7 core sharing

DOI: 10.1021/jacs.5b09466
J. Am. Chem. Soc. 2015, 137, 15809−15816

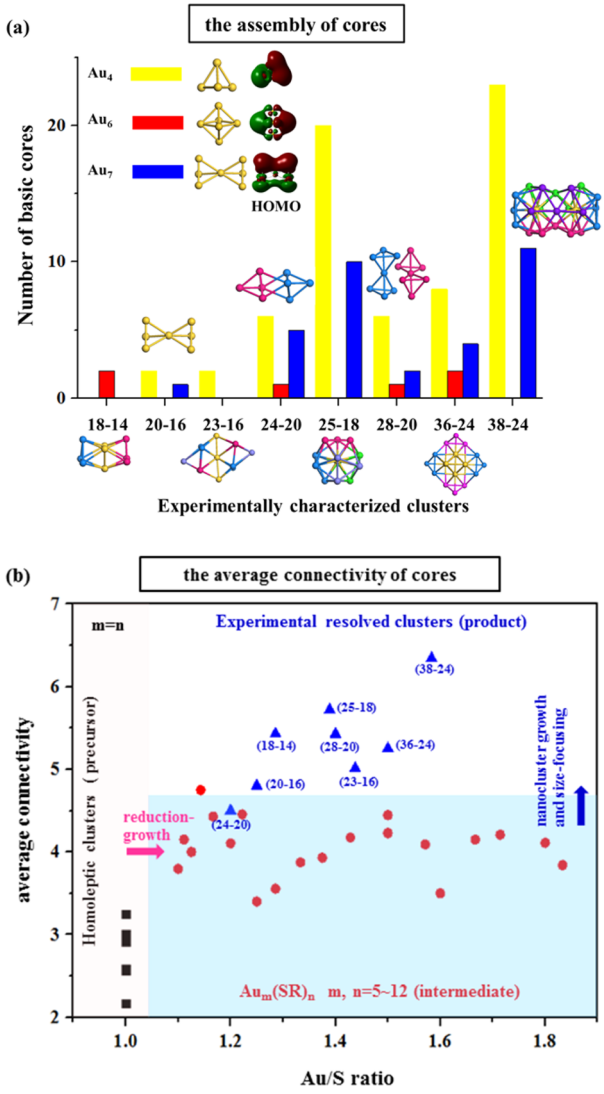

Figure 5. (a) The diverse assembly pattern of inner Au cores. The diverse colors are used to distinguish different basic units in the same inner cores. (b) The calculated average connectivity for each core in different types of precursors, intermediates, and products.

the same edge with each other and followed by sharing the common vertex with Au_6 cores. This phenomena is also observed in the structure of $Au_{36}(SR)_{24}$ as well as $Au_{24}(SR)_{20}$, etc., the only difference is the diverse assembling manner.

We also calculated the populations of the basic Au_4–Au_7 cores in clusters with atomic precise structure in experiment through both molecular substructure miner (MoSS) software[39] and the homemade codes based on the root-mean-square deviation (RMSD) of structural subunits. The underlying algorithm in MoSS software defines different embeddings of one substructure in a single large graph as points in a graph called overlap graph of the substructure and puts an edge between every two equivalent embeddings.[40] Subsequently, the MoSS software can compute the support (or frequency) of a subgraph of a single large input graph to avoid repeated count for one subgraph. Notably, the MoSS software is purely based on the topological connectivity, and some unideal substructures are also counted in certain cases. To avoid such problems, we further wrote a code on the basis of RMSD, and the flowchart of the homemade code is manifested as Scheme S1. The results from the MoSS software and the homemade code are shown in Figure 5a and Table S1, respectively. Both methods predict the dominant building blocks are the Au_4 and Au_7 cores, which also represent two typical core structures within "intermediates". Similarly, by comparing the structure of $Au_{20}(SR)_{16}$, $Au_{28}(SR)_{20}$ and $Au_{36}(SR)_{24}$, Jin et al. reached the conclusion that vertex-sharing bitetrahedral Au_7 core is the basic unit for these three clusters.[16] Also, the tetrahedral Au_4 was presumed to be the common core unit for the small-sized RS-AuNPs with relatively low Au/S ratio.[41] According to our results, the Au_4 and Au_7 basic cores have already been formed within "intermediates" rather than the final "products", validating the previous presumption. Considering that the Au_7 could be formed through two Au_4 core sharing the common vertex, the Au_4 may be viewed as the basic unit in core structure. Moreover, the Au_4 tetrahedron was proposed as a superatom unit that possesses 2 e^- and could form the final clusters with stable electronic structure through a sophisticated network.[23] As shown in Figure 5a, the highest occupied molecular orbitals (HOMOs) of Au_4, Au_6, and Au_7 basic units also exhibit high delocalization. A sequential reduction-growth process: 2 e^- → 4 e^- → 6 e^- → 8 e^- starting from the Au(I)-SR complex to $Au_{25}(SR)_{18}^-$ was proposed from a recent experiment.[29] The initial 2 e^- intermediates were identified as $Au_{11}(SR)_9$ and $Au_{15}(SR)_{13}$, which were both predicted to possess tetrahedral Au_4 core. This successive 2 e^- growth may be caused by the successive addition of Au_4 inner core and finally results in the icosahedral Au_{13} core that can be taken as the fusion of four Au_4 cores. Considering that the 8 e^- in $Au_{25}(SR)_{18}^-$ is also decomposed into four 2 e^- units within each Au_4 superatom, the factors of geometry and electronic structure are evidently interrelated.

With a closer look at the searched intermediates, we also find the 0 e^- → 2 e^- → 4 e^- → 6 e^- growth from $Au_6(SR)_6$ to $Au_8(SR)_6$ to $Au_{10}(SR)_6$ and finally to $Au_{12}(SR)_6$. Along with an increase of Au atom, the inner core evolves from linear Au_2 to tetrahedral Au_4 → vertex-sharing bitetrahedral Au_7 → double vertex-sharing tritetrahedral Au_{10}, as shown in Figure 1a, which demonstrates the successive Au_4 accumulation along with successive 2 e^- growth. To summarize, the Au_4 is indeed the basic unit from both structural and electronic structural viewpoints, and the inner cores within "intermediates" could serve as the building blocks for further growth and size-focusing in the next stage.

Looking back at Figure 1, one can find that the cores in these "intermediate" RS-AuNPs are quite open and hence subjected to the structural deformation, which makes these intermediates highly reactive to participate in the further growth. From this aspect, we calculated the average connectivity of Au atom for RS-AuNPs in different types, with the results illustrated in Figure 5b. According to Figure 5b, the evident increase in average connectivity from the homoleptic "precursors" to the small-sized "intermediates" indicates the preliminary nucleation. Also, given the fact that the average connectivity of the searched ones is lower than the ones in "product", it is evident that these "transition" clusters are less stable and prone to further nucleation as well as growth to achieve higher stability, namely, the experimental "nanocluster (NC) growth" and "size-focusing" stage.[30] Also, the "intermediate" clusters in different sizes possess diverse structural elements, especially in the inner core. Being functioned as building blocks in the following growth and size-focusing process, different sized "intermediate" clusters with varied basic cores may correspondingly produce final "products" with diverse cores.

DOI: 10.1021/jacs.5b09466
J. Am. Chem. Soc. 2015, 137, 15809–15816

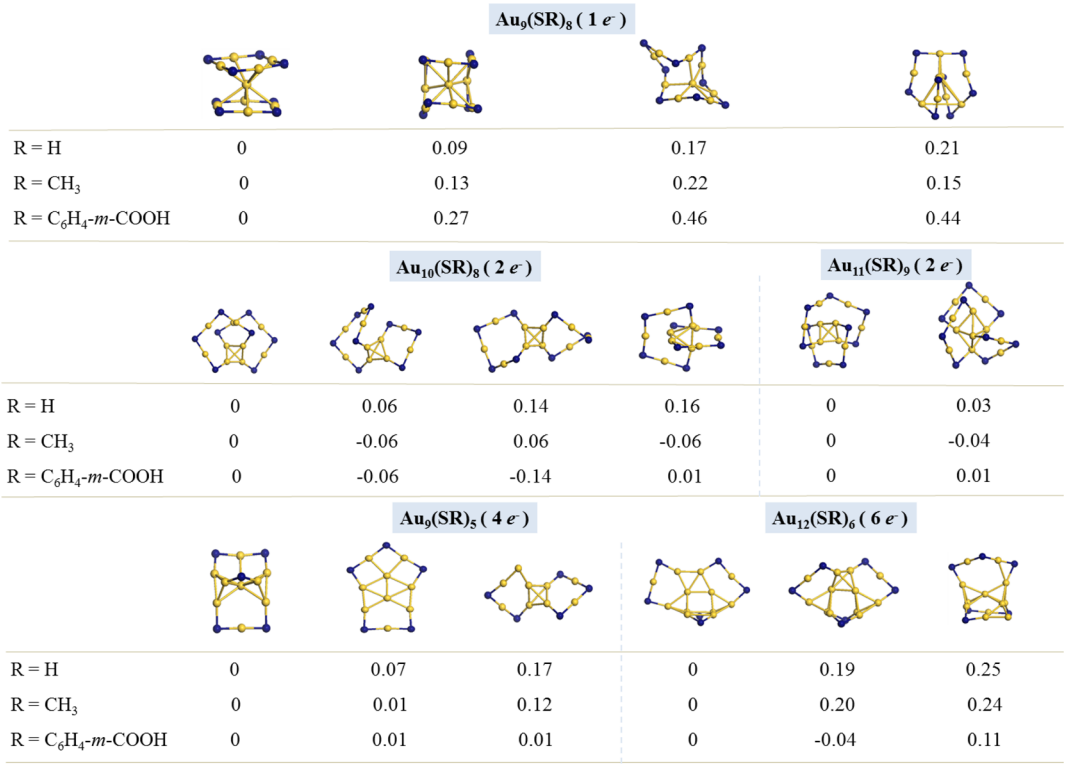

Figure 6. Relative energy (in units of eV) of low-lying isomers for the selected $Au_m(SR)_n$ clusters with R = H, CH_3, C_6H_4-*m*-COOH, respectively.

3.3. The Influence of the Ligands. Recently, both experimentalists and theorists showed that the thiolate ligand of RS-AuNPs may affect the cluster in diverse ways, such as changing the relative stability of isomers and tuning the size and structure in the synthesis.[42−44] In our preliminary exploration of the size evolution of RS-AuNPs, the simplified R = H model was used for reducing the computational costs. Now, the R = CH_3 (commonly used in previous computations) and another realistic model R = C_6H_4-*m*-COOH (*m*-MBA, used in ref 29) were further employed for the DFT calculations of the isomer stability of several selected clusters. The relative energies of the low-lying isomers are listed in Figure 6, with the optimized structures displayed in Supporting Information. It can be found that the substitution of ligands does not change much the structure of inner cores and the Au−S framework for the studied systems. As shown in Figure 6, the X-cone-shaped isomer of $Au_9(SR)_8$ is predicted to be the most stable structure no matter what kind of −SR ligand is introduced. The replacement of different R groups in ligand also exerts little influence on the relative stability of 2 e^- $Au_{11}(SR)_9$, 4 e^- $Au_9(SR)_5$, and 6 e^- $Au_{12}(SR)_6$ clusters, in which the tetrahedral Au_4, vertex-sharing bitetrahedral Au_7 and double vertex-sharing tritetrahedral Au_{10} are still the favored core types, respectively (Figure 6). Although the involvement of R = *m*-MBA in $Au_{10}(SR)_8$, $Au_{11}(SR)_9$, and $Au_{12}(SR)_6$ slightly perturbs the order of relative energy between the low-lying isomers, the energy difference between different isomers is so small (within 0.06 eV) that these isomers are assumed to be equally stable. When the cluster size increases, however, the relative stability and structure of nanoclusters were demonstrated to be sensitive to the variation of ligand structures.[44] The significant ligand effect was indeed shown for the larger-sized $Au_{24}(SR)_{20}$ cluster, for which the substitution of ligand caused about 1 eV energy difference between isomers.[43] Since the number of energetically degenerate isomers is increased in the large-sized $Au_m(SR)_n$ nanoclusters and their structures are affected by the subtle change of thiolate ligand, both the minimum energy path and metastable-transition route are necessary to understand the growth mechanism of nanoparticles. Further study on the ligand effect of the other clusters along the size evolution is still underway in our lab.

4. CONCLUSION

In summary, the structures of a number of intermdiate $Au_m(SR)_n$ (with *m* and *n* ranging from 5 to 12) are resolved by the basin-hopping algorithm combined with genetic algorithm. These transition RS-AuNPs exhibit the core-stacked framework, and the cluster structure is controlled by the number of the gold atoms and thiolates. A preliminary nucleation behavior starting from homoleptic gold thiolates is observed, followed by a gradual growth in both the inner core and staple motifs with the addition of Au atoms and thiolates, respectively. Furthermore, we find that the Au cores of the experimentally resolved clusters are composed of Au_4−Au_7 units within intermediate clusters, in which the Au_4 and Au_7 are the major building units with significant populations. Moreover, the size-sensitive and reactive intermediates prone to participate in the further growth and size-focusing process finally generate the diverse products. The whole size-evolution trend partially rationalizes the initial kinetically controlled “reduction-growth”, the following nanocluster growth, and thermodynamically controlled size-focusing stages in experiment. This work advances the knowledge of fundermental nucleation and growth mechanism of the RS-AuNPs, which is critical for designing new synthetic routes and the practical development in the future.

DOI: 10.1021/jacs.5b09466
J. Am. Chem. Soc. 2015, 137, 15809−15816

■ ASSOCIATED CONTENT

Supporting Information

The Supporting Information is available free of charge on the ACS Publications website at DOI: 10.1021/jacs.5b09466.

Definition of connectivity; the flowchart for calculating the substructure and the results; the binding energy of intermediates; the computational reaction energy of the formation of $Au_{11}(SR)_9$; the optimized structures (R = H); and the low-lying isomers for some selected $Au_m(SR)_n$ clusters with R = H, CH_3, C_6H_4-*m*-COOH, respectively (PDF)

■ AUTHOR INFORMATION

Corresponding Authors

*majing@nju.edu.cn

*ypnku78@gmail.com

Notes

The authors declare no competing financial interest.

■ ACKNOWLEDGMENTS

J.M. is supported by the National Natural Science Foundation of China (grant nos. 21290192, and 21273102). We are grateful to the High Performance Computing Center of Nanjing University for doing the quantum chemical calculations in this paper on its IBM Blade cluster system. Y.P. is supported by the Natural Science Foundation of China (grant nos. 21373176, 21422305), Hunan Provincial Natural Science Foundation of China (12JJ1003), and Scientific Research Fund of Hunan Provincial Education Department (13A100).

■ REFERENCES

(1) Chen, Y. S.; Choi, H.; Kamat, P. V. *J. Am. Chem. Soc.* **2013**, *135*, 8822.

(2) Jin, R. *Nanoscale* **2010**, *2*, 343.

(3) Qian, H. F.; Zhu, M. Z.; Wu, Z. K.; Jin, R. C. *Acc. Chem. Res.* **2012**, *45*, 1470.

(4) Zhang, X. D.; Chen, J.; Luo, Z.; Wu, D.; Shen, X.; Song, S. S.; Sun, Y. M.; Liu, P. X.; Zhao, J.; Huo, S.; Fan, S.; Fan, F.; Liang, X. J.; Xie, J. *Adv. Healthcare Mater.* **2014**, *3*, 133.

(5) Zhang, X. D.; Luo, Z.; Chen, J.; Shen, X.; Song, S.; Sun, Y.; Fan, S.; Fan, F.; Leong, D. T.; Xie, J. *Adv. Mater.* **2014**, *26*, 4565.

(6) Pei, Y.; Zeng, X. C. *Nanoscale* **2012**, *4*, 4054.

(7) Wu, Z.; MacDonald, M. A.; Chen, J.; Zhang, P.; Jin, R. *J. Am. Chem. Soc.* **2011**, *133*, 9670.

(8) Yuan, X.; Zhang, B.; Luo, Z.; Yao, Q.; Leong, D. T.; Yan, N.; Xie, J. *Angew. Chem., Int. Ed.* **2014**, *53*, 4623.

(9) Jadzinsky, P. D.; Calero, G.; Ackerson, C. J.; Bushnell, D. A.; Kornberg, R. D. *Science* **2007**, *318*, 430.

(10) Crasto, D.; Malola, S.; Brosofsky, G.; Dass, A.; Hakkinen, H. *J. Am. Chem. Soc.* **2014**, *136*, 5000.

(11) Das, A.; Li, T.; Li, G.; Nobusada, K.; Zeng, C.; Rosi, N. L.; Jin, R. *Nanoscale* **2014**, *6*, 6458.

(12) Das, A.; Li, T.; Nobusada, K.; Zeng, C.; Rosi, N. L.; Jin, R. *J. Am. Chem. Soc.* **2013**, *135*, 18264.

(13) Das, A.; Li, T.; Nobusada, K.; Zeng, Q.; Rosi, N. L.; Jin, R. *J. Am. Chem. Soc.* **2012**, *134*, 20286.

(14) Qian, H. F.; Eckenhoff, W. T.; Zhu, Y.; Pintauer, T.; Jin, R. C. *J. Am. Chem. Soc.* **2010**, *132*, 8280.

(15) Zeng, C.; Li, T.; Das, A.; Rosi, N. L.; Jin, R. *J. Am. Chem. Soc.* **2013**, *135*, 10011.

(16) Zeng, C.; Liu, C.; Chen, Y.; Rosi, N. L.; Jin, R. *J. Am. Chem. Soc.* **2014**, *136*, 11922.

(17) Zhu, M.; Aikens, C. M.; Hollander, F. J.; Schatz, G. C.; Jin, R. *J. Am. Chem. Soc.* **2008**, *130*, 5883.

(18) Dass, A.; Theivendran, S.; Nimmala, P. R.; Kumara, C.; Jupally, V. R.; Fortunelli, A.; Sementa, L.; Barcaro, G.; Zuo, X.; Noll, B. C. *J. Am. Chem. Soc.* **2015**, *137*, 4610.

(19) Jupally, V. R.; Dass, A. *Phys. Chem. Chem. Phys.* **2014**, *16*, 10473.

(20) Zeng, C.; Qian, H.; Li, T.; Li, Gl; Rosi, N. L.; Yoon, B.; Barnett, R. N.; Whetten, R. L.; Landman, U.; Jin, R. *Angew. Chem., Int. Ed.* **2012**, *51*, 13114.

(21) Chen, S.; Wang, S.; Zhong, J.; Song, Y.; Zhang, J.; Sheng, H.; Pei, Y.; Zhu, M. *Angew. Chem., Int. Ed.* **2015**, *54*, 3145.

(22) Pei, Y.; Gao, Y.; Zeng, X. C. *J. Am. Chem. Soc.* **2008**, *130*, 7830.

(23) Cheng, L. J.; Yuan, Y.; Zhang, X. Z.; Yang, J. L. *Angew. Chem., Int. Ed.* **2013**, *52*, 9035.

(24) Walter, M.; Akola, J.; Lopez-Acevedo, O.; Jadzinsky, P. D.; Calero, G.; Ackerson, C. J.; Whetten, R. L.; Gronbeck, H.; Hakkinen, H. *Proc. Natl. Acad. Sci. U. S. A.* **2008**, *105*, 9157.

(25) Jin, R. C.; Qian, H. F.; Wu, Z. K.; Zhu, Y.; Zhu, M. Z.; Mohanty, A.; Garg, N. *J. Phys. Chem. Lett.* **2010**, *1*, 2903.

(26) Liu, C.; Li, G.; Pang, G.; Jin, R. *RSC Adv.* **2013**, *3*, 9778.

(27) Yu, Y.; Yao, Q.; Luo, Z.; Yuan, X.; Lee, J. Y.; Xie, J. *Nanoscale* **2013**, *5*, 4606.

(28) Jiang, D. E.; Overbury, S. H.; Dai, S. *J. Am. Chem. Soc.* **2013**, *135*, 8786.

(29) Luo, Z.; Nachammai, V.; Zhang, B.; Yan, N.; Leong, D. T.; Jiang, D. E.; Xie, J. *J. Am. Chem. Soc.* **2014**, *136*, 10577.

(30) Yu, Y.; Luo, Z. T.; Yu, Y.; Lee, J. Y.; Xie, J. P. *ACS Nano* **2012**, *6*, 7920.

(31) Iwamatsu, M.; Okabe, Y. *Chem. Phys. Lett.* **2004**, *399*, 396.

(32) Srinivas, M.; Patnaik, L. M. *Ieee Transactions on Systems Man and Cybernetics* **1994**, *24*, 656.

(33) Perdew, J. P.; Burke, K.; Ernzerhof, M. *Phys. Rev. Lett.* **1996**, *77*, 3865.

(34) Delley, B. *J. Chem. Phys.* **1990**, *92*, 508.

(35) Delley, B. *J. Chem. Phys.* **2000**, *113*, 7756 DMol3 4.4 is available from Accelrys..

(36) Shao, N.; Pei, Y.; Gao, Y.; Zeng, X. C. *J. Phys. Chem. A* **2009**, *113*, 629.

(37) Jiang, D.-E.; Whetten, R. L.; Luo, W.; Dai, S. *J. Phys. Chem. C* **2009**, *113*, 17291.

(38) Pei, Y.; Shao, N.; Li, H.; Jiang, D.-E.; Zeng, X. C. *ACS Nano* **2011**, *5*, 1441.

(39) Borgelt, C. *MoSS - Molecular Substructure Miner*; Version 2.11; 2015.3.28; http://www.borgelt.net/moss.html.

(40) Fiedler, M.; Borgelt, C. Proceedings of the 2007 IEEE International Conference on Data Mining, Omaha, NE, October 28−31, 2007; IEEE: New York, 2007; p 399.

(41) Pei, Y.; Pal, R.; Liu, C.; Gao, Y.; Zhang, Z.; Zeng, X. C. *J. Am. Chem. Soc.* **2012**, *134*, 3015.

(42) Zeng, C.; Chen, Y.; Kirschbaum, K.; Appavoo, K.; Sfeir, M. Y.; Jin, R. *Sci. Adv.* **2015**, *1*, e1500045.

(43) Tang, Q.; Ouyang, R.; Tian, Z.; Jiang, D.-E. *Nanoscale* **2015**, *7*, 2225.

(44) Chen, Y.; Zeng, C.; Liu, C.; Kirschbaum, K.; Gayathri, C.; Gil, R. R.; Rosi, N. L.; Jin, R. *J. Am. Chem. Soc.* **2015**, *137*, 10076.